Phase-resolving wave modeling for the wave characterization of coastal and nearshore Marine Renewable Energy sites

Audrey Varing*, Jean-François Filipot*, Volker Roeber†, Fabien Leckler‡, Rui Duarte*, Bertrand Michard§ and Matthias Delpey¶
*France Energies Marines, Brest, France
E-mail: audrey.varing@ite-fem.org
†Tohoku University, Sendai, Japan
‡SHOM, Brest, France
§CEREMA, Plouzané, France
¶Rivages Pro Tech, SUEZ Eau France, Bidart, France

***Abstract*—Marine Renewable Energy (MRE) systems require detailed information regarding the wave induced loads. This paper studies the ability of a phase-resolving model to provide wave information required by MRE applications in coastal and nearshore areas. The phase-resolving approach provides an improved description of the nonlinear wave field found in shallow waters. This approach may also produce other hydrodynamic variables that could benefit the MRE deployment such as the wave height distribution or the wave-induced currents. A dataset collected at a French potential wave energy site allows for model performances quantification. However due to their high computational cost, phase-resolving models are usually used for the simulation of wave packets or short duration wave events and they cannot provide climatologies needed for deriving proper statistics on the seasonal or inter-annual variability of the wave power. Such long term time series are provided by phase-averaged models. This paper aims at drawing attention on the potential benefit of coupling complementary wave modeling strategies (phase-averaged and phase-resolving approaches) to provide advanced wave information to the MRE actors.**

***Index Terms*—Wave resource characterization, Marine Renewable Energy, Phase-resolving wave modeling, Nearshore waves, Nonlinearity.**

I. Introduction

Marine renewable energy (MRE) represents a huge potential for providing electricity worldwide [1]. The MRE industry is a growing sector which has seen important developments over the recent years, including the deployment of pilot and industrial grid-connected MRE farms. Both design optimization and exploitation of MRE systems require detailed information regarding the wave induced loads. All MRE devices, including wind, tidal, wave or ocean thermal energy converters are submitted to waves that also affect their peripheral components like the static and dynamic cables or electric substations. The need for a refined waves description is obvious when considering wave energy harvesting, but waves also induce long term cyclic fatigue on all MRE systems [2], [3]. These energy converters and peripheral systems must further be designed to resist extreme waves events. Finally, wave conditions control the marine operations required to deploy and maintain the MRE devices. Most of the MRE farms are likely to be deployed in coastal or nearshore waters for ease of access, reduced cable expenses and to minimize electricity losses. In these coastal and nearshore waters, waves are a fundamental process exciting the entire water column. Waves interact with the bottom which drives a number of physical processes including shoaling, refraction, reflection, increase in wave skewness and asymmetry [4], dissipation by bottom friction and breaking, and development of infragravity waves [5]. In these shallow environments, waves may also generate strong currents, such as undertows and rip currents with velocity magnitude with the order of 1 m/s [6], [7].

Wave characterization for MRE applications has been extensively addressed in a number of studies through wave resource assessment performed with phase-averaged spectral models [8]–[10]. These studies have provided valuable information regarding the identification of the most profitable wave energy sites through the analysis of global wave parameters such as the wave energy flux, significant wave height or peak period. The wave field in these studies was considered at a global or regional scale, however there was no discussion regarding the validity of the wave model ability to simulate wave fields at a MRE-site scale and to capture the physical processes controlling wave evolution in coastal or nearshore waters.

In this context, the present study aims to assess the capability of a phase-resolving model to provide classical wave parameters (significant wave height, peak period and direction) and also additional wave information for MRE applications such as wave nonlinearities, infragravity waves or wave-induced currents. This modeling approach is applied to the Esquibien site, Audierne Bay, Finistère, France (Figure 1) that has been identified as a potential wave energy site in the framework of the EMACOP research project [11]. Field data of a Datawell wave buoy and two pressure sensors are exploited for model performance assessment. The goal of this study is not to assess the wave resource at the study site (study

already conducted in [11]) but rather to discuss the capability of an existing wave modeling approach to conduct a proper wave characterization to provide guidance for MRE engineers.

The paper starts with the description of the study site, the field experiment and the observational dataset. We then describe the phase-resolving model BOSZ [12] that has been selected for the present study. The model performance evaluation is discussed in section IV. We end the paper with a conclusion on the limitations and capabilities of this phase-resolving model for MRE applications.

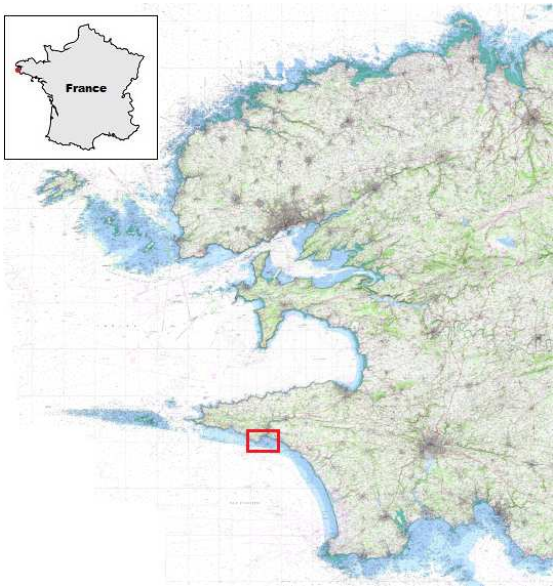

Figure 1. Finistere map. The location of the study is indicated by the red dot on France map and the red square on Finistère map [13].

II. Study site and field experiment

A. Study site

The site has been selected in the framework of the EMACOP project which investigates the opportunity of equipping breakwaters with onshore wave energy converters (WEC) along the French coasts [11]. In this context, Esquibien has been spotted as a potential wave energy site. This area is characterized by a 400 m long breakwater facing south. As shown in Figure 2, the breakwater is connected to a gently sloping platform extending offshore surmounted by shoals and bordered by headlands both focusing the wave energy in complex manners. Esquibien is mainly exposed to wave-systems coming from the Atlantic ocean. Based on the 19-year HOMERE database [15], the wave climate analysis in approximately 20 m water depth in front of the breakwater, gives an averaged significant wave height, peak wave period and peak direction of 1.4 m, 11.5 s and $230°N$ respectively. The Esquibien area is dominated by a semi-diurnal macro-tidal regime with tides ranging from 2 m in neap tide to 6 m in spring tide conditions.

B. Field experiment

To improve knowledge on wave conditions and resource at the site, CEREMA and France Energies Marines deployed a Datawell buoy and two OSSI pressure sensors in front of the breakwater during the winter of 2013-2014 (Figure 2). The wave buoy was located 1.5 km offshore Esquibien breakwater at a depth of 16 m, Chart datum. Two OSSI pressure sensors were placed along a line perpendicular to the breakwater. OSSI 1 was installed at the foot of the breakwater, while OSSI 2 was deployed about 100 m offshore of the breakwater in about 1 m and 8 m water depth, Chart datum respectively.

The Datawell buoy measured significant wave heights fluctuating from 0.5 m to 5 m, peak wave periods ranging from 5 s to 17 s, while the peak wave direction remained relatively constant at $235°N$ as a result of the influence of the bathymetry on the wave field. The OSSI sensors recorded pressure signal continuously at a 5-Hz sampling frequency. We determined the water level based on a hydrostatic hypothesis. We then derived wave elevation spectra from pressure spectra computed from 30-minute pressure samples Fast Fourier Transformed over 512 points, using 50%-overlapping Hann windows which leads to 35 degrees of freedom. From visual inspection, we chose to cut the wave elevation spectra at 0.3 Hz.

In the present study we focus on the December 2013 period that was marked by a wide range of wave conditions.

III. Modeling approach

A. Phase-resolving wave model

Different phase-resolving wave propagation models have been developed during the last decades such as the mild-slope equation and Boussinesq-type equations [16]. Numerical models based on the Boussinesq-type formulation have proved their usefulness to accurately represent nearshore processes [17] and they are often preferred to the mild-slope formulation because of their ability to accurately calculate diffraction, shoaling, refractions and nonlinearity. The standard Boussinesq-type equations for variable water depth were first derived by [18]. [19] extended these standard Boussinesq-type equations to obtain a practical tool to simulate the nonlinear transformation of irregular, multi-directional waves in water of varying depth prior to wave breaking.

In nearshore and coastal waters, waves are strongly affected by the bottom and they develop nonlinear features that lead to wave breaking. Wave breaking is an important modeling issue. Therefore, researchers have developed semi-empirical approaches to account for wave breaking in Boussinesq-type models. A popular approach is the concept of eddy viscosity [20]–[24]. The eddy viscosity-type formulation is capable of modeling the turbulent mixing and dissipation caused by wave breaking. Another common approach is the surface roller concept [25]–[27]. This concept introduces a non-uniform velocity profile, and models the effect of wave breaking by an additional convective momentum term. The cross-shore evolution of short-wave motions, including wave breaking, has been extensively studied with Boussinesq-type models

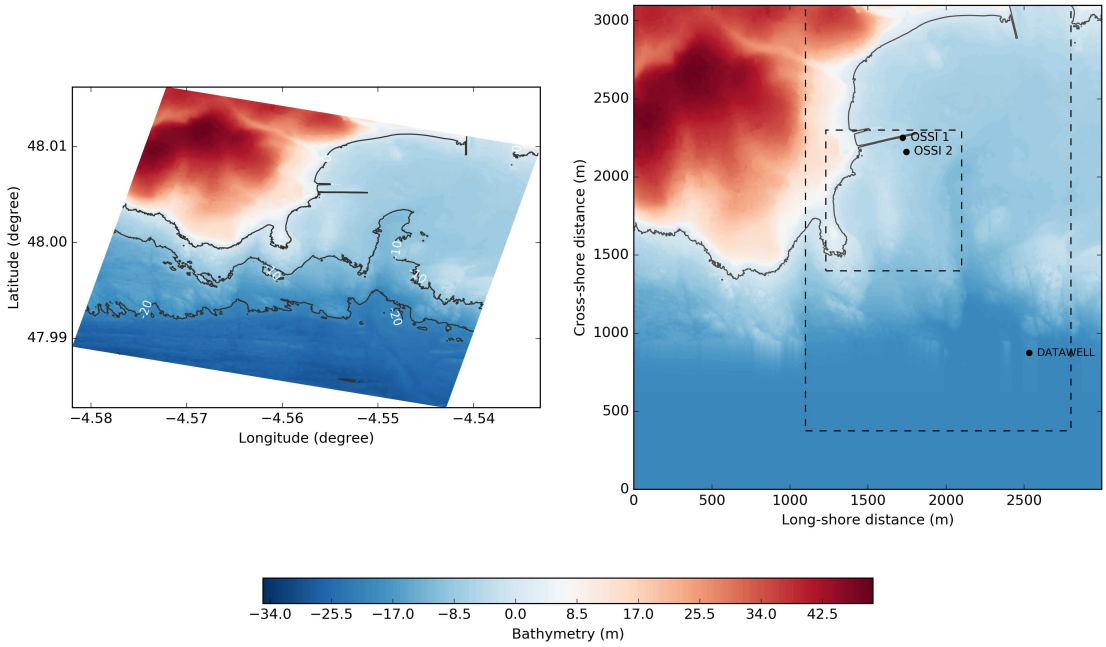

Figure 2. Study site bathymetry from LITTO3D [14] and BOSZ entire computational domain in geographic coordinates (left panel). On the right panel, the sensors locations are visible as black dots. In addition, the black dotted lines indicate the areas extracted from the entire computational domain and retained for plotting and results analysis.

[22], [26], [28] while infragravity motions have been little investigated so far [29], [30]. In the present study, we use the BOSZ model [12] which is described in more details in the next section.

B. The BOSZ model

The Boussinesq Ocean and Surf Zone model, BOSZ, developed by [12] includes depth-integrated equations from the Boussinesq-type equations of Nwogu [19]. These equations have been reformulated to handle nearshore processes such as wave breaking. This model takes into account wave breaking through momentum conservation with primary energy dissipation based on a Riemann solver. From a numerical point of view, a Godunov-type scheme integrates the evolution variables in time. BOSZ equations retain terms of the order of $O(\varepsilon, \mu^2)$, where ε and μ define the nonlinearity and the frequency dispersion parameters respectively. Details of the numerical formulation can be found in [12], [31] and [32]. Due to their computational cost, this type of models are for now restricted to the simulations of single wave events (typically 30 minutes to one hour).

BOSZ was originally applied to energetic waves in a fringing reef environment. [32] provides comprehensive validation of BOSZ with laboratory and field data corresponding to both continental and tropical island conditions. The BOSZ model has been applied to continental conditions in Brittany, France in [33]. It was able to capture the main hydrodynamic processes such as refraction, shoaling, and wave breaking, but also second-order processes such as wave setup and the inherent recirculation in the surf zone. BOSZ has also proven to be a stable and accurate model for irregular bathymetry locations and extreme wave conditions [34].

C. Model setup

The present domain includes Esquibien bay as well as a portion of the open ocean (Figure 2, left panel). The selected rectangular computational domain covers a region of 3000 m (long-shore, x-direction) by 3100 m (cross-shore, y-direction) visible in Figure 2, right panel. The spatial resolution is $\Delta x = 2.5$ m and $\Delta y = 1.25$ m. The bathymetry is extracted from the seamless digital terrain model LITTO3D [14]. The bottom roughness effect on the wave field is taken into account by using a Manning coefficient of 0.025, typical of rough rock seabed [35]. Individual waves are generated along the southern boundary by an internal wavemaker generating waves through a source function approach. The water outside the 20 m-contour is assumed to have a uniform depth of 20 m for a better implementation of the internal wavemaker. Sponge layers on all sides of the domain absorb the outgoing wave energy.

A moderate energetic event on December 18 at 01:15 is modeled and analyzed in this study. The hindcast regional model HOMERE [15] provides the spectral characteristics of the input wave conditions. According to the HOMERE database this event is characterized by a significant wave height (Hs) of 2.31 m, a peak period (Tp) of 14.3 s and a peak wave direction (θ_p) of $238°N$ associated to a spreading angle (s) of 20.4°. The water level is set to 0.52 m. The input frequency-direction spectrum is determined from the spectral parameters described above with a TMA frequency spectrum [36]. The maximum frequency of the input spectrum depends on the dispersive properties of the governing equations and

the spatial resolution. BOSZ governing equations present good dispersion accuracy up to $kh = 2\pi$ with kh the dimensionless wavenumber. The cut-off frequency of the input spectrum is set to 0.24 Hz as the model cannot handle the propagation of short-dispersive waves. Harmonics higher than 0.24 Hz do not contain significant energy in the input spectrum to affect the overall performance of the model. The normalized directional distribution $E(\theta)$ is defined as:

$$E(f,\theta) = A\ cos^{2s}\left(\frac{(\theta-\theta_p)}{2}\right) \quad (1)$$

where parameter A is a normalization coefficient, s is the directional width parameter and θ_p is the peak direction [37]. The normalized directional distribution is symmetric about the peak direction, and narrower for larger s.

The BOSZ model utilizes OpenMP for parallel processing within a computing node. The numerical model uses a Courant number of 0.5 preventing the fastest waves from traversing more than one grid cell within a time step under breaking wave conditions [32]. The total runtime of BOSZ is 45 minutes to properly develop the offshore and nearshore sea state. It requires 2.5 days of computation with 8 processors. The last 30 minutes of the simulations are used for results analysis.

IV. Results

In the present study, we exploit the sea surface elevation and the sea surface orbital velocities to derive different wave statistics and parameters.

A. BOSZ output field

1) Wave by wave field description: Figure 3 presents a snapshot of the sea surface elevation from BOSZ outputs. This type of figure could not be provided by a spectral model. At the boundary, the incoming waves have a south-west direction. Their orientation changes due to the refraction process induced by the bathymetry variation. In the vicinity of the breakwater, a superposition of incident and reflected waves appears. The waves are reflected by the breakwater and the coastline (Figure 3, right panel).

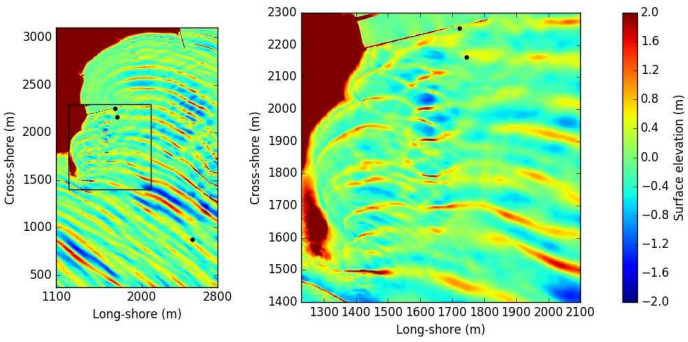

Figure 3. Snapshot of the sea surface elevation from BOSZ simulation with the input direction $238°N$. These areas are extracted from the entire computational domain presented in Figure 2.

2) Significant wave height field description: The significant wave height is calculated from the sea surface elevation variances $S(f)$ as follows:

$$Hs = 4\sqrt{\int_0^{0.3Hz} S(f)df} \quad (2)$$

Though the input spectrum has a cut-off frequency of 0.24 Hz, higher frequency waves are free to develop during propagation in the domain. Since there is no significant energy above 0.3 Hz, this frequency is taken as upper limit to compute the significant wave height.

Figure 4 presents the significant wave height on the domain. Extensive wave height variations are visible, particularly in front of the breakwater. With the incoming swell direction, the breakwater is partly situated in the shadow of the island on the left of the domain. As observed on the sea surface elevation snapshot (Figure 3), the incoming swell is submitted to refraction because of the water depth variations. In front of the breakwater, wave height variations are observed at equally spaced locations corresponding to half the wave length in the area. This pattern is due to the interferences between incident and reflected waves that generate standing waves characterized by nodes and anti-nodes.

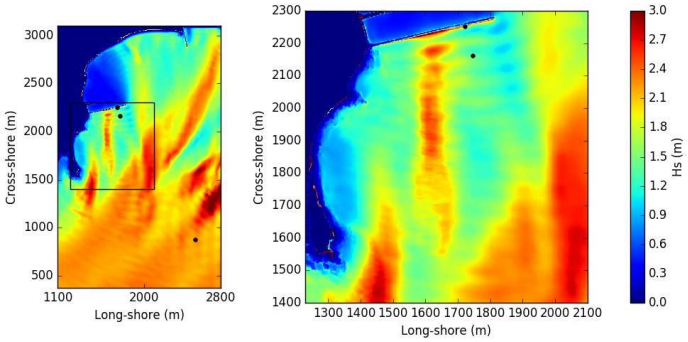

Figure 4. Significant wave height from BOSZ simulation with the input direction $238°N$. These areas are extracted from the entire computational domain presented in Figure 2.

3) Wave-induced current field description: An important aspect of the model is the capacity of modeling mean wave-induced currents at each point of the domain. Because the water level is fixed during the simulation, the tidal current cannot be computed from BOSZ. The ability to model tidal change and then resolve tidal currents is a feature that needs to be improved with such models. This is a challenge for phase-resolving models. Figure 5 represents the mean wave-induced current of the simulation with the input direction $238°N$. The colors indicate the intensity of the current and the arrows show the directions. The right panel of Figure 5 indicates the presence of strong wave-induced currents around the island which are generated by substantial wave breaking according to the model. The wave-induced current follows the coastline towards the north and along the breakwater. Offshore of the breakwater, the current seems to be impacted by the complex bathymetry on the right of the domain with a shoal zone.

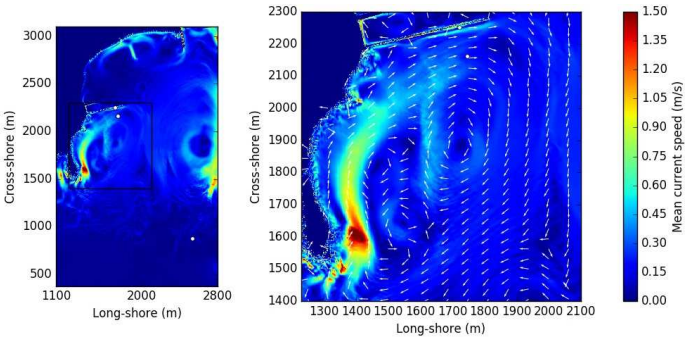

Figure 5. Wave-induced current map from BOSZ simulation with the input direction $238°N$. These areas are extracted from the entire computational domain presented in Figure 2. The left panel presents the intensity of the wave-induced current. The right panel presents the intensity and the normalized direction (white arrows) of the wave-induced current around the breakwater.

B. BOSZ output at observations location

1) Elevation spectra: Further analysis is required to compare the model outputs and the observations. The elevation spectra are computed from the sea surface elevation at the three sensor locations and compared to the observed spectra. At the Datawell location, close to the offshore boundary, Figure 6 shows that the predicted spectrum agrees with the observations. The energy associated to the peak frequency f_p is well represented but differences are visible at higher frequencies. When the waves reach the pressure sensor OSSI 2, they have propagated toward the shore in shoaling waters. They have undergone transformations because of the changing topography that causes refraction and shoaling. Nonlinear effects are also important and transform the wave spectra. At OSSI 2, cross-spectral energy transfers from the peak frequncy, induce energy growth of lower and higher frequencies. Transfer of energy to higher frequencies is an indication of wave skewness and asymmetry growth [38], and is an important process controlling the breaking onset. As shown in Figure 6, while the observations present a generation of harmonics around a frequency of $2f_p$, the model computes an energy growth at a frequency smaller than $2f_p$. It is noted that, the total energy at OSSI 1 is higher than OSSI 2. Though dissipation could have been expected during the waves propagation between these two locations, the standing waves pattern visible in Figure 4 might explain the trend described by both the observations and the model. The observed spectral energy density at the foot of the breakwater (OSSI 1) shows that between OSSI 1 and OSSI 2, the energy associated with the higher harmonics has vanished while the main peak and the infragravity band energy (frequencies below 0.05 Hz) have significantly grown. This trend is also obvious in the BOSZ spectrum though the energy at the peak and in the infragravity band is highly overestimated. It is noted that the modeled subharmonic frequencies deviate from the observations. A plausible explanation can be related to the width of the modeled spectral peak which is larger than the observed peak at each sensor. The energy growth due to triad interactions at subharmonic f_{sh} are due to interaction of two peak components [39] f_1 and f_2 such that $f_{sh} = f_2 - f_1$. For the same central peak frequency f_p, if the spectral peak width increases (hence the difference $f_2 - f_1$), the frequency f_{sh} increases in return, which seems to happen at OSSI 1 and OSSI 2.

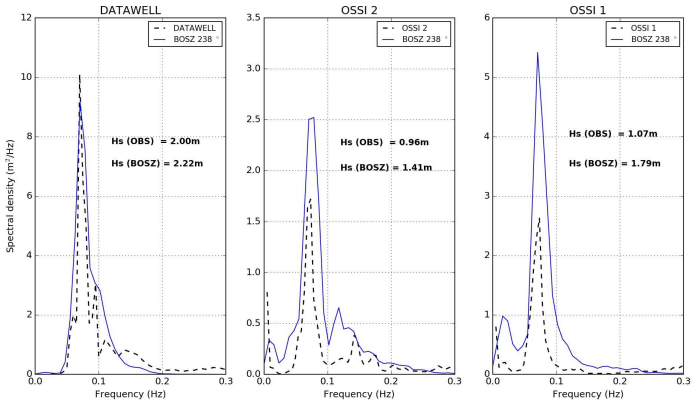

Figure 6. Spectra of sea surface elevation of BOSZ simulation with the input direction $238°N$ compared to the observations at the sensors locations, along with the associated significant wave height values.

2) Probability Density Function of the Elevation: The Probability Density Function of the Elevation (PDFE) is calculated at the pressure sensors and Datawell locations for the simulation and the observations (Figure 7). The PDFE at the Datawell location presents relatively good agreement between the predicted and measured data. However, there are larger differences at the OSSI locations. The model overestimates the high waves and underestimates the small waves compared to the observations. Figure 6 shows that BOSZ tends to overestimate the wave energy at OSSI 1 and OSSI 2 which explains why BOSZ produces higher elevations than expected in Figure 7 at OSSI 1 and OSSI 2.

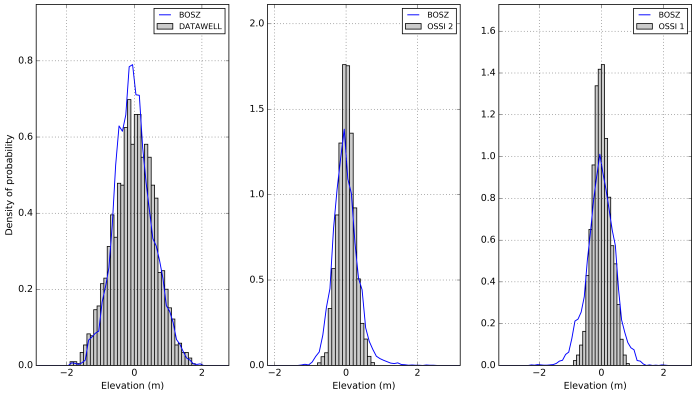

Figure 7. Probability density function of sea surface elevation of BOSZ simulation with the input direction $238°N$ compared to the observations at the sensors locations.

3) Wave power: The wave power could have been calculated on the whole domain by using an equation based on integral parameters and using the approximation of deep water.

However, it is not valid in the shallow waters of the present area. The wave power per unit crest length P is then calculated from the following equation which uses the wave spectrum components:

$$P = \frac{\rho g^2}{4\pi} \int_0^\infty \frac{S(f)}{f} \left[\left(1 + \frac{2k_f d}{sinh(2k_f d)} \right) tanh(k_f d) \right] df \quad (3)$$

where ρ is the seawater density, g is the acceleration due to gravity and d is the water depth. k_f is the wave number given by the dispersion relation, as follows:

$$(2\pi f)^2 = g k_f \ tanh(k_f d) \quad (4)$$

The wave power per unit crest length is computed at the sensor locations and compared to the observations (Table I). Equation 3 is then used only at some specific location instead of the whole domain, since the calculation of the wave spectrum at every location of the computational domain is a time-consuming process. It is observed in Table I that the wave power is overestimated by the model at the three locations. Strong differences are seen closer to the breakwater. These errors are due to the overestimation already seen in the wave energy spectra in Figure 6.

Table I
WAVE POWER PER UNIT CREST LENGTH DETERMINED FROM EQUATION 3 FOR THE DIFFERENT BOSZ SIMULATIONS AND THE OBSERVATIONS.

P (kW/m)	Datawell	OSSI 2	OSSI 1
Observation	23.8	4.1	3.5
BOSZ (238°)	32.4	8.8	9.7

C. Sensitivity analysis

Sensitivity analyses were carried out to explore the effect of (1) the input wave direction and (2) the input tide level on the simulation results. We expected that these two parameters would strongly influence the wave dynamics in this area. Although other parameters may impact the output results of the model (input spectrum shape, friction coefficient, ...), no sensitivity analysis was carried out to explore their effects.

1) Input wave direction: In order to study the sensitivity of the model to the input wave direction, simulations are performed with the input directions $234°N$ and $242°N$. They correspond to a change of $+/-4°$ on the direction provided by the HOMERE database ($238°N$) on the studied case in sections IV-A and IV-B. Such variations in direction may be caused by uncertainties from the HOMERE database. Figure 8 presents the different elevation spectra associated to the different input directions and the observations at the Datawell and pressure sensors locations. Changing the input direction by a few degrees, has almost no influence on the spectra at the Datawell location, whereas it induces strong differences in the spectra at the pressure sensor locations. With the input direction $234°N$, the wave are coming more from the south of the bay and the spectral density close to the breakwater is more overestimated than with the original direction. On the contrary, with the input direction $242°N$, the wave energy is less overestimated than with the other simulations. Table II shows the relative errors between the observed and modeled significant wave height determined with equation 2. As observed in Figure 8 and according to Table II, the input wave direction $242°N$ provides results more in agreement with the observations. For the remaining of the study, results from the simulation with the input wave direction $242°N$ will be considered.

From the tests on the input wave direction, it is deduced that the BOSZ model is sensitive to that parameter. The choice of the input wave peak direction and therefore the entire input spectrum need to be carefully addressed.

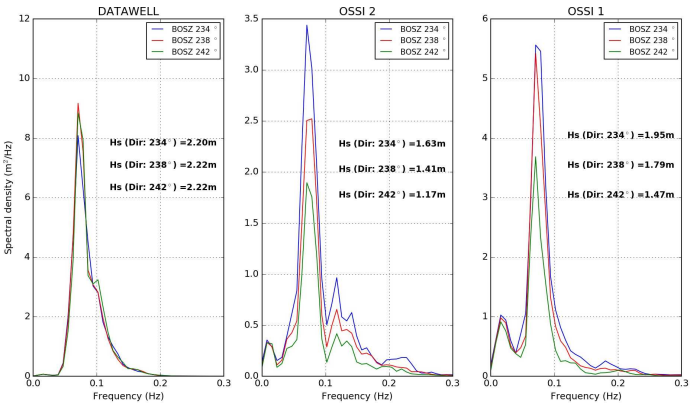

Figure 8. Sea surface elevation spectra of BOSZ simulations with the input directions $234°N$, $238°N$ and $242°N$ along with the associated significant wave height values.

Table II
SIGNIFICANT WAVE HEIGHT RELATIVE ERRORS CALCULATED BETWEEN THE DIFFERENT BOSZ SIMULATIONS AND THE OBSERVATIONS

Hs relative error (%)	Datawell	OSSI 2	OSSI 1
BOSZ (234°)	-10	-69	-82
BOSZ (238°)	-11	-46	-67
BOSZ (242°)	-11	-22	-37

2) Input tidal level: Since the tidal level is fixed during a simulation, the sensitivity of the model to the input water level (WL) is analyzed. Simulations with approximately $+/-50$ cm from the original situation (input wave direction $242°N$ and $WL = 0.52$ m) are performed. Figure 9 provides the elevation spectra from these different simulations at the Datawell and OSSI locations. With the lower tidal level ($WL = 0$ m), the total energy and the spectral peak energy is higher in every locations than the other simulations. The energy of the higher and lower harmonics are also more important. What seems more likely is that because simulation $WL = 0$ m has less water, the waves feel the bottom more and shoaling is more significant. The total energy is then higher than simulations with a higher water level. Increasing the tidal level to 1 m has the opposite effect. Because there is more water, there is

certainly less shoaling and the total energy is smaller than with the simulations $WL = 0.52$ m and $WL = 0$ m.

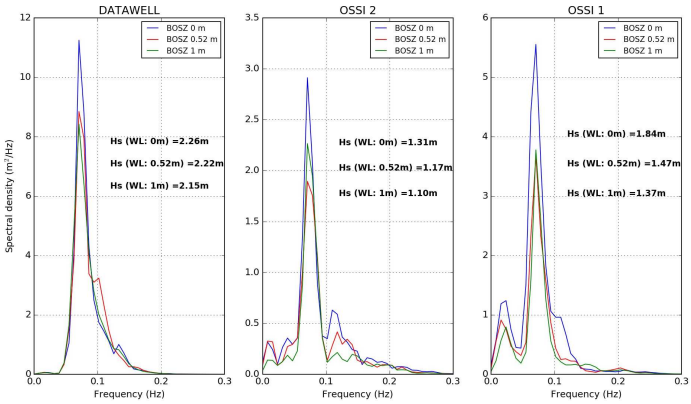

Figure 9. Sea surface elevation spectra of BOSZ simulations with the input tidal levels $0m$, $0.52m$ and $1m$ along with the associated significant wave height values.

V. Conclusion

This study investigates the ability of a phase-resolving model to capture the most relevant wave information in the context of MRE applications.

On the documented event in this paper, BOSZ produces wave elevation statistics that could not be provided by a spectral wave model. These statistics are difficult to predict especially in coastal and nearshore areas because of the enhanced waves nonlinearity causing the statistics to strongly deviate from the classical Gaussian or Rayleigh laws [40]. Wave induced currents determined by BOSZ are valuable information for the MRE sector. BOSZ also provides information on the nonlinear evolution of the wave spectrum from the offshore buoy to the pressure sensors deployed at the foot of the breakwater. Though there are disagreements between the observed and modeled spectra, the BOSZ model is able to capture the nonlinear wave energy growth. Further efforts will be required to obtain a better quantitative representation of these nonlinear wave transformations. Since difference are already observed at the Datawell spectrum, improvement could be made to the wave input spectrum. As the sensitivity analysis on the input wave direction revealed, the input wave spectrum must be carefully selected. Progress should include the reconstruction of a spectrum from the wave buoy data and its implementation in the code. With a better representation of the energy offshore, it is expected that closer to the breakwater the high frequency tail of the spectra will be better in agreement with the observations. This study also reveals that the BOSZ model is sensitive to tidal level. This will motivate the improvement of the model to take into account the water level fluctuations. These future improvement will help provide more reliable wave power information to MRE engineers.

The approach presented in this paper provides wave information at small spatial scales that are complementary to classical spectral model analysis to develop a more detailed methodology for wave characterization of MRE projects. Wave climatologies are essential at the early stages of a resource assessment [41], [42] and nearshore nonlinear wave transformations provided by a phase-resolving model are a useful complement for engineers to better study the response of MRE structures (loads, fatigue) in shallow water waves. Combined with a spectral model, the BOSZ model could provide advanced hydrodynamic processes required for the latest stages of wave resource assessment [43]. Future studies with BOSZ should include improving the wave breaking process parameterization that affects the wave energy resource estimation and analyzing extreme wave conditions. Other sites should also be analyzed to determine the sensitivity of the simulations to the zone of study. These statements open new fields of research and will motivate future studies to define innovative methodologies on the coupling of phase-averaged spectral and phase-resolving approaches in the objective of providing optimal wave information to the Marine Renewable Energy sector.

Acknowledgment

This work has benefited from government support managed by the Agence Nationale de la Recherche under the program Investissement d'Avenir with the reference ANR-10-IEED-0006-14.

References

[1] R. Pelc and R. M. Fujita, "Renewable energy from the ocean," *Marine Policy*, vol. 26, no. 6, pp. 471–479, 2002.

[2] P. R. Thies, L. Johanning, and G. H. Smith, "Assessing mechanical loading regimes and fatigue life of marine power cables in marine energy applications," *Proceedings of the Institution of Mechanical Engineers, Part O: Journal of Risk and Reliability*, p. 1748006X11413533, 2011.

[3] I. A. Milne, "An experimental investigation of turbulence and unsteady loading on tidal turbines," Ph.D. dissertation, ResearchSpace@ Auckland, 2014.

[4] J.-F. Filipot, "Investigation of the bottom-slope dependence of the nonlinear wave evolution toward breaking using swash," *Journal of Coastal Research*, 2015.

[5] T. H. C. Herbers, S. Elgar, and R. T. Guza, "Infragravity-frequency (0.005-0.05 Hz) motions on the shelf. part II: free waves," *J. Phys. Oceanogr.*, vol. 25, pp. 1063–1079, 1995. [Online]. Available: http://ams.allenpress.com/archive/1520-0485/25/6/pdf/i1520-0485-25-6-1063.pdf

[6] R. A. Dalrymple, "A mechanism for rip current generation on an open coast," *Journal of Geophysical Research*, vol. 80, no. 24, pp. 3485–3487, 1975.

[7] M. Delpey, F. Ardhuin, P. Otheguy, and A. Jouon, "Effects of waves on coastal water dispersion in a small estuarine bay," *Journal of Geophysical Research: Oceans*, vol. 119, no. 1, pp. 70–86, 2014.

[8] A. M. Cornett *et al.*, "A global wave energy resource assessment," in *The Eighteenth International Offshore and Polar Engineering Conference*. International Society of Offshore and Polar Engineers, 2008.

[9] J. C. van Nieuwkoop, H. C. Smith, G. H. Smith, and L. Johanning, "Wave resource assessment along the cornish coast (uk) from a 23-year hindcast dataset validated against buoy measurements," *Renewable energy*, vol. 58, pp. 1–14, 2013.

[10] D. Mediavilla and H. Sepúlveda, "Nearshore assessment of wave energy resources in central chile (2009–2010)," *Renewable Energy*, vol. 90, pp. 136–144, 2016.

[11] B. Michard, E. Cosquer, A. Mallégol, J. Coignard, G. Amis, J.-F. Filipot, K. A. Kpogo-Nuwoklo, M. Olagnon, F. Ropert, and P. Sergent, "Emacop project: characterising the wave energy resources of hot spots in brittany for onshore wec," in *Proceedings of the 11th European Wave and Tidal Energy Conference*, 2015.

[12] V. Roeber, "Boussinesq-type model for nearshore wave processes in fringing reef environment," Ph.D. dissertation, Honolulu, University of Hawaii at Manoa, 2010.
[13] "Geoportail," https://www.geoportail.gouv.fr/, accessed: 2017-04-20.
[14] Y. Pastol, C. Le Roux, and L. Louvart, "Litto d-a seamless digital terrain model," *The International hydrographic review*, vol. 8, no. 1, 2007.
[15] E. Boudière, C. Maisondieu, F. Ardhuin, M. Accensi, L. Pineau-Guillou, and J. Lepesqueur, "A suitable metocean hindcast database for the design of marine energy converters," *International Journal of Marine Energy*, vol. 3, pp. e40–e52, 2013.
[16] P. L.-F. Liu and I. J. Losada, "Wave propagation modeling in coastal engineering," *Journal of Hydraulic Research*, vol. 40, no. 3, pp. 229–240, 2002.
[17] E. Rusu and C. G. Soares, "Modeling waves in open coastal areas and harbors with phase-resolving and phase-averaged models," *Journal of Coastal Research*, vol. 29, no. 6, pp. 1309–1325, 2012.
[18] D. H. Peregrine, "Long waves on a beach," *J. Fluid Mech.*, vol. 27, pp. 815–827, 1967.
[19] O. Nwogu, "Alternative form of Boussinesq equations for nearshore wave propagation," *J. of Waterway, Port Coast. Ocean Eng.*, vol. 119, no. 6, pp. 618–637, 1993.
[20] J. Zelt, "The run-up of nonbreaking and breaking solitary waves," *Coastal Engineering*, vol. 15, no. 3, pp. 205–246, 1991.
[21] G. Wei, J. T. Kirby, S. T. Grilli, and R. Subramanya, "A fully nonlinear Boussinesq model for surface waves. part 1. highly nonlinear unsteady waves," *J. Fluid Mech.*, vol. 294, pp. 71–92, 1995.
[22] A. B. Kennedy, Q. Chen, J. T. Kirby, and R. A. Dalrymple, "Boussinesq modeling of wave transformation, breaking, and runup. i: 1d," *Journal of waterway, port, coastal, and ocean engineering*, vol. 126, no. 1, pp. 39–47, 2000.
[23] Q. Chen, J. T. Kirby, R. A. Dalrymple, A. B. Kennedy, and A. Chawla, "Boussinesq modeling of wave transformation, breaking, and runup. ii: 2d," *Journal of Waterway, Port, Coastal, and Ocean Engineering*, vol. 126, no. 1, pp. 48–56, 2000.
[24] P. J. Lynett, T.-R. Wu, and P. L.-F. Liu, "Modeling wave runup with depth-integrated equations," *Coastal Engineering*, vol. 46, no. 2, pp. 89–107, 2002.
[25] I. A. Svendsen, "Wave heights and set-up in a surf zone," *Coastal Eng.*, vol. 8, pp. 303–329, 1984.
[26] H. A. Schäffer, P. A. Madsen, and R. Deigaard, "A boussinesq model for waves breaking in shallow water," *Coastal Engineering*, vol. 20, no. 3-4, pp. 185–202, 1993.
[27] P. A. Madsen, O. Sørensen, and H. Schäffer, "Surf zone dynamics simulated by a boussinesq type model. part i. model description and cross-shore motion of regular waves," *Coastal Engineering*, vol. 32, no. 4, pp. 255–287, 1997.
[28] M. Tonelli and M. Petti, "Shock-capturing boussinesq model for irregular wave propagation," *Coastal Engineering*, vol. 61, pp. 8–19, 2012.
[29] P. Madsen and O. Sørensen, "Bound waves and triad interactions in shallow water," *Ocean Engineering*, vol. 20, no. 4, pp. 359–388, 1993.
[30] P. A. Madsen, O. Sørensen, and H. Schäffer, "Surf zone dynamics simulated by a boussinesq type model. part ii: Surf beat and swash oscillations for wave groups and irregular waves," *Coastal Engineering*, vol. 32, no. 4, pp. 289–319, 1997.
[31] V. Roeber, K. F. Cheung, and M. H. Kobayashi, "Shock-capturing boussinesq-type model for nearshore wave processes," *Coastal Engineering*, vol. 57, no. 4, pp. 407–423, 2010.
[32] V. Roeber and K. F. Cheung, "Boussinesq-type model for energetic breaking waves in fringing reef environments," *Coastal Engineering*, vol. 70, pp. 1–20, 2012.
[33] J.-F. Filipot, V. Roeber, M. Boutet, C. Ody, C. Lathuiliere, S. Louazel, F. Ardhuin, A. Lusven, M. Outré, S. Suanez *et al.*, "Nearshore wave processes in the iroise sea: field measurements and modelling," in *Proceedings of the 7th International Conference on Coastal Dynamics 2013*, no. http://www. coastaldynamics2013. fr/pdf_files/055_Filipot_Jean_Francois. pdf, 2013.
[34] N. Li, V. Roeber, Y. Yamazaki, T. W. Heitmann, Y. Bai, and K. F. Cheung, "Integration of coastal inundation modeling from storm tides to individual waves," *Ocean Modelling*, vol. 83, pp. 26–42, 2014.
[35] G. J. Arcement and V. R. Schneider, "Guide for selecting manning's roughness coefficients for natural channels and flood plains," 1989.
[36] S. A. Hughes, "The tma shallow-water spectrum description and applications," DTIC Document, Tech. Rep., 1984.
[37] L. H. Holthuijsen, "Observations of the directional distribution of ocean wave energy," *J. Phys. Oceanogr.*, vol. 13, pp. 191–207, 1983. [Online]. Available: http://ams.allenpress.com/pdfserv/10.1175%2F1520-0485(1983)013%3C0191%3AOOTDDO%3E2.0.CO%3B2
[38] S. Elgar and R. Guza, "Observations of bispectra of shoaling surface gravity waves," *Journal of Fluid Mechanics*, vol. 161, pp. 425–448, 1985.
[39] Y. Eldeberky, "Nonlinear transformation of wave spectra in the nearshore zone," Ph.D. dissertation, Delft UNiversity of Technology, Netherlands, 1996.
[40] Y. Wu, D. Randell, M. Christou, K. Ewans, and P. Jonathan, "On the distribution of wave height in shallow water," *CE*, vol. 111, pp. 39–49, 2016.
[41] A. Akpınar and M. İ. Kömürcü, "Assessment of wave energy resource of the black sea based on 15-year numerical hindcast data," *Applied Energy*, vol. 101, pp. 502–512, 2013.
[42] H. C. Smith, D. Haverson, and G. H. Smith, "A wave energy resource assessment case study: Review, analysis and lessons learnt," *Renewable Energy*, vol. 60, pp. 510–521, 2013.
[43] M. Folley, A. Cornett, B. Holmes, P. Lenee-Bluhm, and P. Liria, "Standardising resource assessment for wave energy converters," in *Proceedings of the 4th International Congress on Ocean Energy, Dublin, Ireland*, 2012.